Non-destructive single-pass low-noise detection of ions in a beamline

Stefan Schmidt,[1,2] Tobias Murböck,[3] Zoran Andelkovic,[4] Gerhard Birkl,[3] Wilfried Nörtershäuser,[1] Stefan Stahl,[5] and Manuel Vogel[4]

[1]*Institut für Kernphysik, Technische Universität Darmstadt, 64289 Darmstadt, Germany*
[2]*Institut für Kernchemie, Johannes Gutenberg–Universität Mainz, 55099 Mainz, Germany*
[3]*Institut für Angewandte Physik, Technische Universität Darmstadt, 64289 Darmstadt, Germany*
[4]*GSI Helmholtzzentrum für Schwerionenforschung, 64291 Darmstadt, Germany*
[5]*Stahl Electronics, 67582 Mettenheim, Germany*

We have conceived, built, and operated a device for the non-destructive single-pass detection of charged particles in a beamline. The detector is based on the non-resonant pick-up and subsequent low-noise amplification of the image charges induced in a cylindrical electrode surrounding the particles' beam path. The first stage of the amplification electronics is designed to be operated from room temperature down to liquid helium temperature. The device represents a non-destructive charge counter as well as a sensitive timing circuit. We present the concept and design details of the device. We have characterized its performance and show measurements with low-energy highly charged ions (such as Ar^{13+}) passing through one of the electrodes of a cylindrical Penning trap. This work demonstrates a novel approach of non-destructive, low noise detection of charged particles which is, depending on the bunch structure, suitable, e.g., for ion traps, low-energy beamlines or accelerator transfer sections. © 2015 AIP Publishing LLC. [http://dx.doi.org/10.1063/1.4935551]

I. INTRODUCTION

Electronic detection of image currents induced by moving charged particles is a versatile tool for non-destructive measurements in various experimental frameworks. Applications comprise Schottky-type electronic pick-ups in storage rings[1–3] and electronic detection in particle traps such as Penning traps, with detection sensitivities ranging down to the single-ion level.[4–6] Many implementations rely on fixed-frequency oscillatory or repetitive signals and work within small frequency bands, which is beneficial for high signal-to-noise ratios. This, however, is not a necessary requirement given a sufficiently noiseless detection technology.

The first quantitative analysis of the electrical current induced in conductors by charged particles moving above their surface was presented by Shockley in 1938.[7] For the purpose of particle detection, such currents need to be suitably picked up and amplified. The underlying principles of application of this technique to stored particle detection and cooling in Penning traps are described, for example, in Refs. 4, 5, and 8–10. In this report, we present a detector formed by one of the cylindrical electrodes of a Penning trap which is pervaded along its central axis by ion bunches that enter the trap. This device is cryogenic-compatible and based on low-noise charge amplification. It has been operated in the framework of the SpecTrap experiment.[11–14] There, it serves both as a charge counter and for delivering timing information. We describe the principles of its operation, details of the technical implementation, and present measurement results.

II. SETUP

The detector is operated in the environment of the SpecTrap open-endcap cylindrical Penning trap, shown in Fig. 1. The trap is designed for precision laser spectroscopy experiments with highly charged ions. A detailed description of this setup can be found in Refs. 12 and 14 and only a brief description will be given here. The ions are produced externally in a compact electron beam ion source (EBIS) and are transported in bunches through a low-energy beamline[15] towards the Penning trap, at energies of a few keV per charge. The trap itself is located in the cold vertical bore of a superconducting magnet with a field strength of 4 T. It consists of a stack of cylindrical electrodes, where the two outmost electrodes are used for dynamic ion capture.

The detector is connected to the outmost electrode at the ion entry side of the trap. It hence detects the charge signals of ion bunches entering the trap and is used both for non-destructive charge detection and for timing information. Thus, the pick-up signal of the incoming ion bunch can be used as a trigger for the capturing process. The detector board and the Penning trap are both mounted on a heat sink, which is attached to a helium dewar for good thermal conductivity (Fig. 1). The detector tests were performed with bunches of Ar^{13+} ions, but the operation principle is obviously independent of the choice of this ion and of the fact that the pick-up electrode is part of a Penning trap.

A. Design of the detector

The low-noise amplifier used in this setup is a highly sensitive device for non-destructive single-pass ion detection. Although designed for use in a cryogenic environment, low temperature is not strictly necessary for the operation of this non-destructive ion detector (NID). An internal regulation and biasing circuitry counteracts temperature-related drift effects. It is built on a cryogenic-compatible epoxy substrate, very similar to standard printboard material, with surface mount
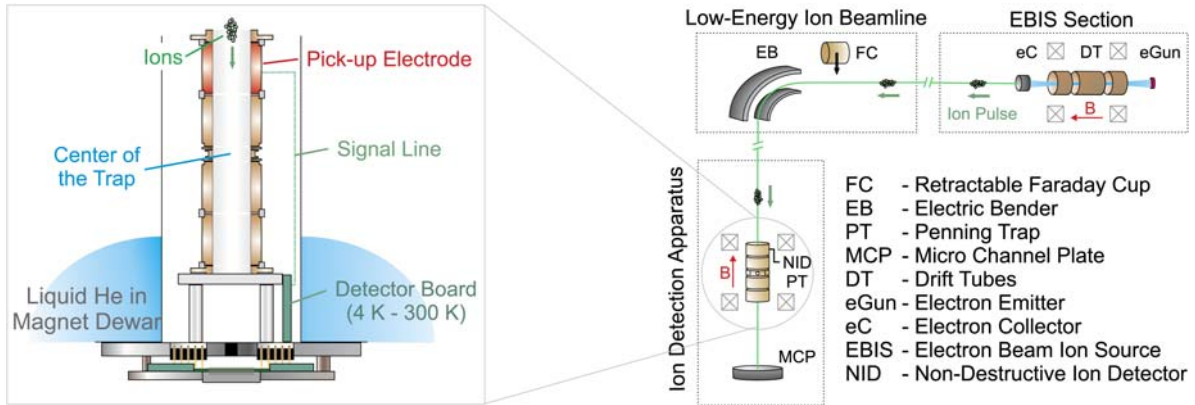
FIG. 1. Schematic overview of the relevant parts of the experimental setup (not to scale). Left: The setup of the Penning trap including the pick-up electrode and the cryo-electronics of the non-destructive ion detector (NID). Right: Pulsed beams of highly charged Ar^{13+} ions are produced in an electron beam ion source (EBIS) and guided through the HITRAP low-energy beamline[15] towards the ion detection section.

(SMD) components soldered on top. The amplifier is tightened with brass screws to ensure good thermal contact when operated at 4.2 K.

The proximity of the amplifier's input to the pick-up electrode minimizes parasitic capacitances, which in turn helps to reach a sensitivity normally not achievable with a remotely located amplifier. As shown in Fig. 2, the circuit structure consists of a high-impedance input stage with a low-noise gallium-arsenide field effect transistor (T1), a cascode stage (T2) to lower the input capacitance, an active load to increase amplification (T3), and a subsequent buffer output stage to meet the cable impedance of the signal line towards the room temperature part of the detection system (75 Ω). The input stage exhibits a voltage amplification of roughly four and amplifies the AC voltage signal at the input $U_i(t)$ which is created by the effective ion image charge $Q_i(t)$ on the effective input capacitance C_{in}: $U_i(t) = Q_i(t)/C_{in}$. Additional voltage amplification of the AC voltage signal is achieved by

use of an external amplifier (Cryo Bias Controller CBC-1, Stahl Electronics) operated at room temperature. C_{in} is the sum of all parasitic capacitances present at the input, given by the capacitance of the pick-up electrode, the capacitance of the leads from the pick-up electrode to the amplifier input, the input capacitance of the amplifier itself, and the protection diodes. The diodes are required to protect the sensitive input stage during the capturing phase of the trap. Here, a high voltage signal is applied rapidly (on the time scale of ns) to the pick-up electrode via the ion capture circuit (Fig. 2). These diodes limit the occurring voltages to safe values around 1 V_{pk}. For stand-alone operation of the detector, e.g., in a beamline, these diodes and the ion capture circuit are superfluous.

The amplifier is mostly made of large-geometry MESFET gallium-arsenide transistors (T1 = NE6510179A; T2,T3 = NE651R479A) as active elements, thin film resistors and polymer as well as standard ceramic C0G capacitors, which all show small temperature dependencies. The choice of
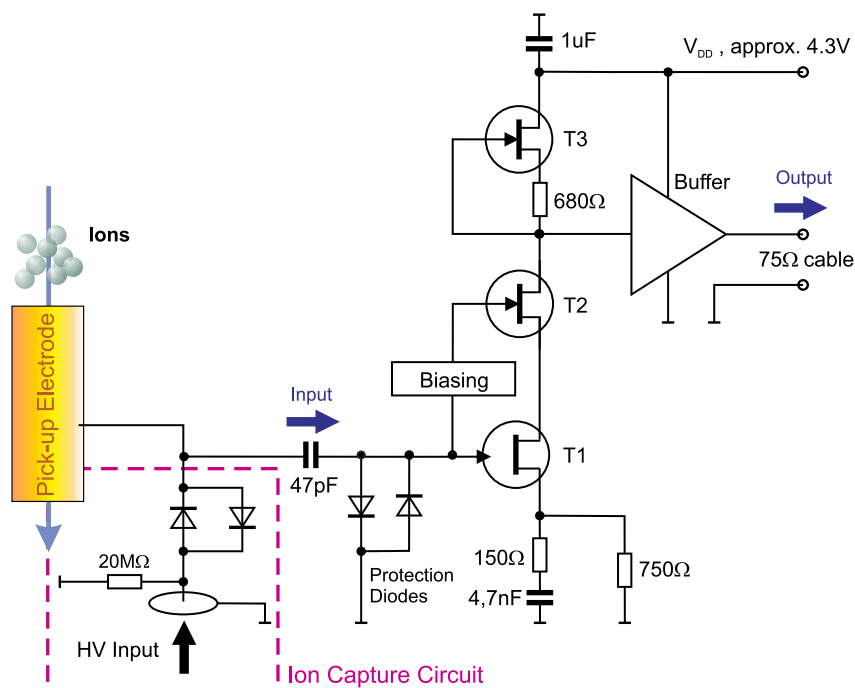

FIG. 2. Circuit diagram of the non-destructive ion detector. See text for details.

these components fulfills the requirements imposed by the experimental objective, which is full cryogenic operability, vacuum compatibility and low noise figures at the frequency range of interest (ROI).

B. Induced charge signal

The charge in the pick-up electrode induced by a point-like particle of charge q is modeled as a function of the axial and radial positions, z and r,[16]

$$
\begin{aligned}
Q_{pl}(z,r) = \frac{q}{\pi R} \int_0^\infty & \frac{I_0(x \cdot \frac{r}{R})}{I_0(x)} \\
& \cdot \left[\mathrm{sinc}\left(x\frac{z-z'}{\pi R}\right)(z-z')\right]_{z'=z_r}^{z'=z_l} dx \\
= q \cdot \Xi(z,r), & \quad\quad\quad\quad\quad (1)
\end{aligned}
$$

where the integral extends over all possible frequency components of the induced signal with x as a suitable integration variable and r the radial position of the point-like particle. Hence, the induced charge signal $Q_{pl}(z,r)$ only depends on the geometry of the electrode, which is described by the geometry function $\Xi(z,r)$. The radius and the length of the electrode are $R = 10.6$ mm and $L = z_r - z_l = 22$ mm, respectively, where z_l and z_r are the boundaries of the electrode. $I_0(x)$ is the modified Bessel function of order zero and $\mathrm{sinc}(x)$ is the normalized cardinal sine function.

Eq. (1) has been evaluated numerically (method: Gauss-Kronrod rule[17]) for different particle positions z and radial positions r. The result is depicted in Fig. 3, where the geometry function $\Xi(z,r)$ is shown as a function of the axial coordinate for different r. The area under each geometry function is equal for different radial positions $r < R$ and is given by the length of the electrode $\int \Xi(z,r)dz = L$. Variations in the area, given by the numerical computation, are only on the ppm level and can thus be neglected.

Eq. (1) is derived from the Poisson equation under the condition that the pick-up electrode is surrounded by two infinitely long cylinders with a constant radius, such that the induced charge on the electrode is not affected by fringe electric fields. Since the ratio between the length of our trap including the surrounding ion optical elements and the diameter of the trap is larger than 10, this condition is met.

In the many-particle case, the ion bunch is described by the charge distribution Γ. It consists of N identical particles, each represented by a δ-function. For simplicity, we assume that the ions are moving along the z-axis ($r = 0$) with the constant velocity v. The induced charge signal in the pick-up electrode $Q_i(t)$ then reads

$$
Q_i(t) = \int \Gamma(vt - z)\Xi(z,0)dz. \quad\quad\quad (2)
$$

In general, the shape of the induced charge signal $Q_i(t)$ depends on the radial distribution of the ions. However, the integrated charge signal $\int Q_i(t)dt$, used to determine the total number of ions per bunch, is independent of the ions' radial position.

III. MEASUREMENTS

A. Frequency response and timing information

To determine the frequency response of the detector, we have applied a test signal at the input stage of the amplifier and have measured the system's response for a wide frequency spectrum at room temperature. The results are shown in Fig. 4. The voltage amplification of the non-destructive ion detector is 3.2 at maximum. The frequency response resembles a bandpass filter in the range $\Delta f = f_2 - f_1$, with $f_1 = 60$ kHz being the lower cutoff frequency (-3 dB point) and $f_2 = 5.5$ MHz being the upper cutoff frequency (-3 dB point). In case of the external room-temperature amplifier, the amplification factor amounts to about 78 with $f_1 = 3$ kHz and $f_2 = 6$ MHz.

The high-pass characteristics of the NID are necessary to decouple the amplifier's input stage from the high voltage input, preventing the amplifier from damages by a permanent high voltage signal. In addition, the high-pass filter reduces the significant $1/f$-noise of the gallium-arsenide field effect transistors (FETs) but also leads to a substantial reduction of the input signal. On the high-frequency end, the low-pass characteristics are chosen for maximum noise reduction, without further reduction of the input signal. It is worthwhile to mention that the NID circuit can be designed with a wide frequency range, allowing the frequency selection to be done externally.[18] This leads to a higher flexibility regarding particular experimental conditions.
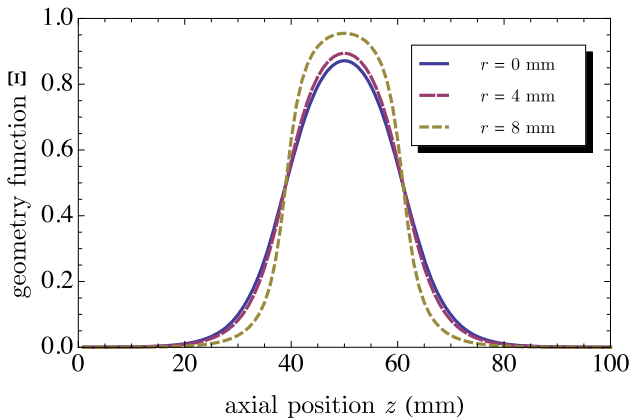

FIG. 3. Geometry function of the pick-up electrode for different radial positions r of a single ion. The center of the electrode is at $z = 50$ mm.
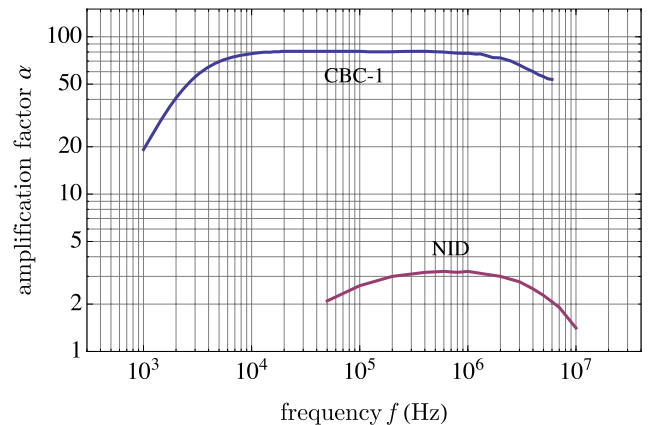

FIG. 4. Frequency response of the non-destructive ion detector (NID) and the Cryo Bias Controller CBC-1 at room temperature.

In addition, we have determined the voltage amplification factor α of the detector at cryogenic temperatures. For liquid nitrogen and liquid helium temperatures, we get $\alpha_{4K} \approx \alpha_{77K} \approx 4$.

As described in Sec. II, the signal of the incoming ion bunch can be used as a trigger for dynamic ion capture in the Penning trap. A quantity describing the response time of this process is the rise time of the induced charge signal. The maximum speed of the amplifier is set by the upper cutoff frequency, limiting the rise time to a minimum value of about 180 ns for the present detector. However, for typical experimental conditions at SpecTrap, the response of the detector is sufficiently fast, due to the temporal extension of the bunch, which is of the order of 1 μs.

B. Effective capacitance and noise density

As already discussed in Sec. II A, the effective input capacitance is predominantly determined by the capacitance of the pick-up electrode C_E. However, also the capacitance of the protection diodes C_D at the HV-input as well as other parasitic capacitances need to be considered. Since the latter cannot be measured directly, they are included in C_E and C_D in the following.

The effective input capacitance has been determined by measuring the system's response when adding a test capacitance of 1 pF to the input of the amplifier. With the measured value for $C_D = (7.8 \pm 0.1)$ pF and $C_E = (34.1 \pm 0.7)$ pF, we find $C_{in} = (49.2 \pm 0.8)$ pF. Here, also an increase of the capacitance of the leads from the pick-up electrode to the amplifier input has been considered, resulting from their proximity to the inner walls of the helium dewar (see Fig. 1). This effect accounts for approximately 17% of the total effective input capacitance and occurs when the trap is attached to the helium dewar.

The noise performance of the detector has been determined by measuring the spectral noise density using a network analyser (HP3598A). Several sweep spectra at different amplifier temperatures were recorded with a resolution bandwidth of 1.2 kHz and a sweep time of 2.82 s with peak detection activated. Fig. 5 shows measured spectra of the input noise density of the amplifier, i.e., the voltage and current fluctuations that are present at the high impedance input stage (T1). Hence, the noise density contains both the input voltage
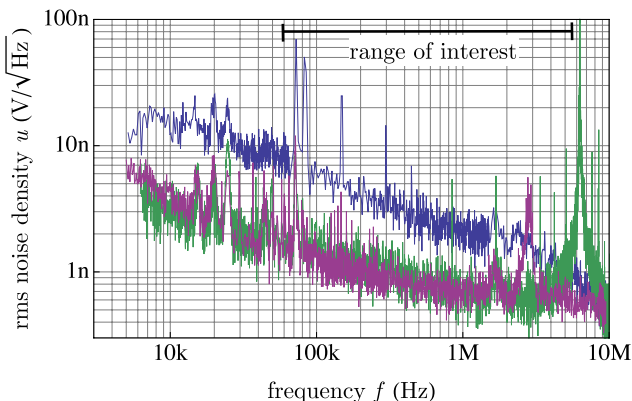

FIG. 5. Root mean square input noise density u of the non-destructive ion detector at 300 K (blue), 77 K (purple), and 4.2 K (green).

noise density and the input current noise density. The spikes in the noise density spectra in the frequency range below 2 MHz are caused by the LCD displays of the Cryo Bias Controller CBC-1 and are thus regarded as external noise sources.

To characterize the total noise level of the amplifier for a given frequency range of interest, we introduce the effective noise amplitude a given by

$$a = \alpha \cdot \sqrt{\sum_{\text{ROI}} u^2 \cdot \delta f}, \tag{3}$$

where δf is the frequency difference between two data points, α the total voltage amplification factor, and u the root mean square (rms) noise density given in Fig. 5. To obtain a good approximation for the effective noise amplitude a, we have chosen the frequency range Δf of the NID as the frequency range of interest. Having a frequency range of 60 kHz to 5.5 MHz, the effective noise amplitude at room temperature amounts to approximately 2.7 mV$_{\text{rms}}$. This sets the limit for the minimum detectable signal and corresponds to a sensitivity of about 16 000 elementary charges (or 1200 ions of charge state 13), if the signal threshold is defined as 4 σ.

As compared to the room temperature measurement, the effective noise amplitude at 77 K is reduced by a factor of 1.5 and amounts to 1.8 mV$_{\text{rms}}$ within the range of interest, resulting in a sensitivity of about 10000 elementary charges. At 4.2 K, we find $a \approx 1.9$ mV$_{\text{rms}}$. The noise density peaks around 3 MHz and 8 MHz at liquid nitrogen and liquid helium temperature, respectively, are caused by oscillations in the amplifier. This leads to an overall increase of the noise level. The reason for these oscillations is not yet identified, but we observed that they disappear from time to time. This as well as a further noise reduction is addressed in our upcoming version of the detector (see Sec. IV). Consequently, at the moment, the best results for the operation of the NID are found at liquid nitrogen temperature, both in terms of noise density and technical requirements for handling cryogenic liquids.

C. Ion number determination

The total number of ions within a single bunch can be calculated by

$$N_{\text{NID}} = \frac{1}{q} \int \Gamma(vt - z)\mathrm{d}z, \tag{4}$$

if the charge distribution $\Gamma(vt - z)$ is known. According to Eq. (2), $\Gamma(vt - z)$ can be determined from the deconvolution of the induced charge signal $Q_i(t)$ and the geometry function $\Xi(z,0)$. This, however, is not necessary since a direct determination of the total number of ions from the voltage signal $U(t) = Q_i(t) \cdot \alpha / C_{in}$ can be done. By use of Eq. (2), the integrated voltage signal can be expressed as

$$\int U(t)\mathrm{d}t = \frac{\alpha}{C_{in}} \int \left(\Xi(z,0) \int \Gamma(vt - z)\mathrm{d}t \right) \mathrm{d}z, \tag{5}$$

such that with Eq. (4) and $\int \Xi(z,r)\mathrm{d}z = L$ the total number of ions is given by

$$N_{\text{NID}} = \frac{1}{q} \frac{v}{L} \frac{C_{in}}{\alpha} \kappa \int U(t)\mathrm{d}t. \tag{6}$$

Here, by introducing the correction factor κ, we have considered that the frequency spectrum of $U(t)$, and thus the signal itself, is reduced by the bandpass filter of the amplifier (NID). The factor κ has been calculated for each signal by modeling its frequency spectrum using a Gaussian profile multiplied by the frequency response of a first-order bandpass filter. The latter has been fitted to the data shown in Fig. 4. Typical values of this factor are $\kappa \approx 1.13$ and have been included in the evaluation.

To verify the results of the non-destructive ion detector, the total number of ions was additionally determined at two different points along the low-energy beamline. The first detection system, a Faraday cup (FC), is placed 2.5 m in front of the non-destructive ion detector, see also Fig. 1 (right). The second detector, a micro-channel plate (MCP), is located 0.9 m behind the trap. The MCP was operated without the presence of a strong electric field (operation voltage) to directly measure the current of the incoming ion bunch using a current-to-voltage amplifier (DHPCA-100, Femto). With the measured voltage signal $U_F(t)$, the total number of ions was determined via

$$N_{MCP} = \int \eta \frac{U_F(t)}{\alpha_F \cdot q} dt, \tag{7}$$

where η is a coefficient that accounts for secondary electron emission or the quantum efficiency of the micro-channel plate. Here, α_F is the amplification factor of the current-to-voltage amplifier. In the present case, η has been determined to be 0.48 ± 0.04 for similar micro-channel plates used in the low-energy beamline. Since a direct measurement of η for the given micro-channel plate was not possible, $\eta = 0.48$ is used as a good estimate in the following.

Typical signals of the non-destructive ion detector (at room temperature) and the micro-channel plate, recorded for different bunch sizes, are shown in Fig. 6. To account for fluctuations of produced particle numbers in the EBIS, the signals of 64 repetitions were averaged. Since the principle of operation of both devices is based on charge counting and charge amplification, saturation effects as well as dead times are not expected for the present setup and signals that are above the noise level are true signals. The kinetic energy of the ions amounts to 545 eV per charge and was determined via a time-of-flight measurement. The asymmetry on the right hand side (the trailing edge) of the ion bunch results from a deceleration
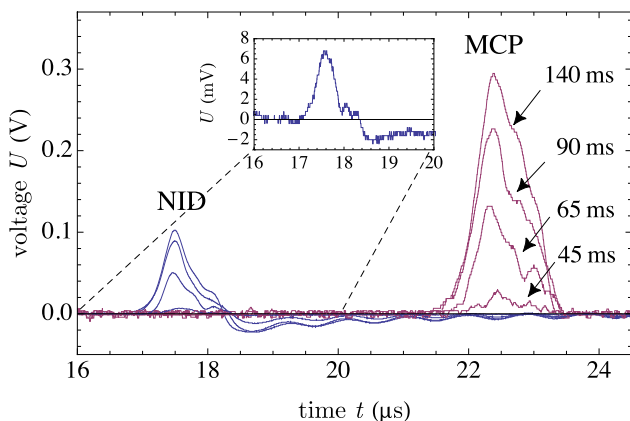
step in which the initial energy of the ions was reduced by approximately 86%.[15] The negative overshoots in the signals of the non-destructive ion detector result from cutting off low frequency parts of the initial signal by the high-pass characteristics of the amplifier. They have been accordingly considered (excluded) in the determination of the total number of ions. Each spectrum was determined with identical beamline settings and the number of ions was changed by varying the charge breeding time in the EBIS. Four different signals are shown with 140 ms, 90 ms, 65 ms, and 45 ms breeding time. Longer breeding results in a larger number of Ar^{13+} ions. The inset shows the signal of the non-destructive ion detector for a breeding time of 45 ms with a different scaling.

In Fig. 7, the experimental results of the total ion number determination in both detection systems are compared directly: The total number of ions detected with the NID is plotted as a function of the total number of ions detected with the MCP. This analysis allows to calibrate the results obtained with the NID and gives information on the transport efficiency of the beamline from the position of the NID to the MCP. Based on the comparative measurements of the total number of ions measured with the FC placed before the bender section and with the MCP, we expect that the data points lie within the green area in this representation. The upper border (FC limit) has been generated with the number of ions detected at the FC, while the lower boarder (MCP limit) corresponds to a transport efficiency of 100% between the NID and MCP positions. Obviously, the FC limit, assuming 100% transport efficiency between the FC and the NID, overestimates our observed number of ions, since ion transport through different sections of the beamline (e.g., the electrostatic bender) is not perfect. The total number of ions determined with the non-destructive ion detector is well within the expected range. In addition, a linear fit to the experimental data (dashed line) is shown, representing a constant transport efficiency of about 57% between the NID and the MCP, in case the ion number determination of the NID can be calibrated as well. This calibration can be verified using the inset of Fig. 7: The transport efficiency between the NID and MCP positions increases for small ion numbers until it reaches almost 100%.

FIG. 6. Averaged ion signals at the non-destructive ion detector (blue) and the multi channel plate (red). See text for details.
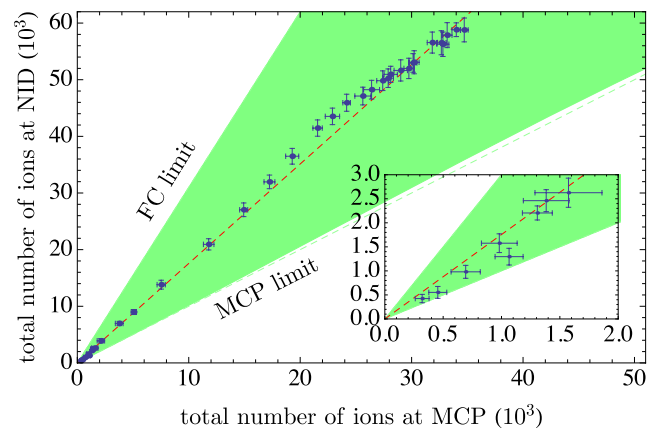

FIG. 7. Comparison between the total number of ions at the non-destructive ion detector (NID) and the micro-channel plate (MCP). The different data points correspond to different breeding times (30 ms–170 ms) and thus different bunch sizes. The measurements were performed without changing the beamline settings.

TABLE I. Overview of the systematic and statistic contributions to the total error budget. The values are given as percentages for two different regimes.

Ion number	Total error (%)	Systematic error (%)	Statistic error (%)
10^5	3	1.6	1.4
10^3	13	1.5	11.5

This confirms our determination of the total number of ions by use of the NID.

At large ion numbers, the detected number of ions slightly deviates from the linear trend. This might be referred to the fact that the aperture of the ion beamline as well as the ion optical settings are favorable for a large number of ions, but there is no obvious explanation for this behavior. The error bar of each data point results from systematic and statistic uncertainties. The uncertainty of the effective capacitance and the reduction of the frequency spectrum of the ion bunch caused by the finite detection bandwidth of the amplifier have been considered as systematic uncertainties. The contribution of the systematic uncertainties to the total error budget depends on the total number of ions and typical values are presented in Table I for two different ion numbers.

The lowest detectable signal represented here corresponds to 320 ions of charge state 13. The bunch length of this signal is about 3 times larger than the length of the electrode, leading to a resolution of approximately 100 ions of charge state 13, equivalent to about 1300 elementary charges. The improved resolution, compared to the value given in Sec. III B, results from the signal averaging and thus the reduced effective noise amplitude of (0.22 ± 0.02) mV$_{rms}$.

IV. CONCLUSION

We have presented the design and operation of a non-destructive charge detector, which is able to detect an ion bunch while it is passing through a pick-up electrode. The measured sensitivity agrees with the expected value, given by the noise properties of our charge detector electronics and it amounts to about 16 000 elementary charges in a single measurement, or 1300 elementary charges if signal averaging can be used. Furthermore, we have shown the feasibility of an absolute ion number determination with our charge detector which is accurate to less than 23% for ion bunches of a few hundreds of ions and less than 4% for ion bunches of around 55 000 ions. The detection bandwidth of 5.5 MHz gives a timing resolution of 180 ns.

In our case, the timing signal facilitates dynamic ion capture in a Penning trap but it can in principle be used for various other applications requiring in-flight non-destructive detection of bunches of charged particles. Depending on the bunch structure, the NID could be used for ion counting and non-destructive monitoring of the ion beam even at much higher energies, e.g., in accelerator transfer sections.

Based on the findings presented in this paper, an advanced version of the detector is currently under construction. A substantial improvement is expected to arise from the use of a novel transistor technology, which is being implemented into our design. High-electron-mobility transistors (HEMTs) have specially been designed and optimized for use at cryogenic temperatures and feature exceptionally low noise at the frequency range of our interest. Samples of these parts have been fabricated for us in a HEMT-process and were optimized for charge detection purposes.[19] The noise level (both voltage and current noise density) of these components is almost one order of magnitude lower than the one of the current device.

[1]S. van der Meer, Rev. Mod. Phys. **57**, 689 (1985).
[2]F. Nolden, P. Hülsmann, Yu. A. Litvinov, P. Moritz, C. Peschke, P. Petri, M. S. Sanjari, M. Steck, H. Weick, J. X. Wu, Y. D. Zang, S. H. Zhang, and T. C. Zhao, Nucl. Instrum. Methods Phys. Res., Sect. A **659**, 69–77 (2011).
[3]M. S. Sanjari, P. Hülsmann, F. Nolden, A. Schempp, J. X. Wu, D. Atanasov, F. Bosch, C. Kozhuharov, Yu. A. Litvinov, P. Moritz, C. Peschke, P. Petri, D. Shubina, M. Steck, H. Weick, N. Winckler, Y. D. Zang, and T. C. Zhao, Phys. Scr. **T156**, 014088 (2013).
[4]D. J. Wineland and H. G. Dehmelt, J. Appl. Phys. **46**, 919–930 (1975).
[5]L. S. Brown and G. Gabrielse, Rev. Mod. Phys. **58**, 233 (1986).
[6]S. Sturm, A. Wagner, M. Kretzschmar, W. Quint, G. Werth, and K. Blaum, Phys. Rev. A **87**, 030501 (2013).
[7]W. Shockley, J. Appl. Phys. **9**, 635–636 (1938).
[8]W. M. Itano, J. C. Bergquist, J. J. Bollinger, and D. J. Wineland, Phys. Scr. **T59**, 106 (1995).
[9]X. Feng, M. Charlton, M. Holzscheiter, R. A. Lewis, and Y. Yamazaki, J. Appl. Phys. **79**, 8–13 (1996).
[10]D. F. A. Winters, M. Vogel, D. M. Segal, and R. C. Thompson, J. Phys. B **39**, 3131 (2006).
[11]M. Vogel, D. F. A. Winters, D. M. Segal, and R. C. Thompson, Rev. Sci. Instrum. **76**, 103102 (2005).
[12]Z. Andelkovic, R. Cazan, W. Nörtershäuser, S. Bharadia, D. M. Segal, R. C. Thompson, R. Jöhren, J. Vollbrecht, V. Hannen, and M. Vogel, Phys. Rev. A **87**, 033423 (2013).
[13]T. Murböck, S. Albrecht, Z. Andelkovic, R. Cazan, V. Hannen, R. Jöhren, J. Vollbrecht, S. Schmidt, D. M. Segal, R. C. Thompson, M. Vogel, Ch. Weinheimer, W. Nörtershäuser, and G. Birkl, Phys. Scr. **T156**, 014096 (2013).
[14]S. Schmidt, Ch. Geppert, and Z. Andelkovic, Hyperfine Interact. **227**, 29–43 (2014).
[15]Z. Andelkovic, N. Kotovskiy, K. König, B. Maaß, T. Murböck, D. Neidherr, S. Schmidt, J. Steinmann, G. Vorobjev, and F. Herfurth, Nucl. Instrum. Methods Phys. Res., Sect. A **795**, 109-114 (2015).
[16]J. Steinmann, Ph.D. thesis, Friedrich-Alexander-Universität Erlangen-Nürnberg (in preparation).
[17]P. J. Davis and P. Rabinowitz, *Methods of Numerical Integration* (Courier Corporation, 2007).
[18]H. Spieler, *Semiconductor Detector Systems* (Oxford University Press, 2005), Vol. 12.
[19]Q. Dong, Y. X. Liang, D. Ferry, A. Cavanna, U. Gennser, L. Couraud, and Y. Jin, Appl. Phys. Lett. **105**, 013504 (2014).